Improvements in approximating-functions method for the optical reflection and transmission problems of nonlinear dielectric layers

Zolotariov D.

Independent researcher. Kharkiv, Ukraine;
ORCID: https://orcid.org/0000-0003-4907-7810 denis@zolotariov.org.ua

Received: 04.02.2022

Abstract. We improve a known approximating-functions method, a special case of finite-element method, in order to solve electrodynamics problems of optical reflection and transmission of one-dimensional layers in time domain, using a Volterra integral-equation technique. The main purpose of this improvement is increasing calculation speed and reducing computer resources, which is especially important for the problems of nonlinear media. The method is validated on the example of reflection and transmission problems arising for three different types of electromagnetic Gaussian-like pulses, which are incident on a material layer with second-order nonlinearity inserted in between linear media.

Keywords: nonlinear dielectric layers, approximating-functions method, Volterra integral-equation method, analytical–numerical methods, computational efficiency.

UDC: 535, 51-73

1. Introduction

Interaction of electromagnetic fields with nonlinear or non-stationary media is of fundamental importance because it describes the key processes in emerging technologies such as optical communications and computers, nanocomputers, etc. In all of these problems, the interactions processes with material media take place in a time domain inside some bounded spatial region. Modelling these initial–boundary problems requires not only development of adequate mathematical models, but also construction of powerful and convenient methods for their solving. The most practical of these techniques are numerical or analytical–numerical approaches.

A Volterra integral-equation method is an approach based on integral equations, which are equivalent to the Maxwell's equations [1, 2]. It has the following important features: natural description of non-stationary and nonlinear features of material media, unified definition of the problems irrespective of inhomogeneity assumption for these media, and inclusion of both initial and boundary conditions in the same equations. A particular form of the appropriate relations is the Volterra integral equation of the second kind. The latter is the same for the media of different types and different laws of variation of their parameters and, moreover, it does not depend on initial electromagnetic signal.

All of these features simplify significantly problem statement and enables universal modelling algorithms for a wide range of electrodynamics problems, many of which have been described in Refs. [3, 4]. The most efficient and promising solution is an analytical–numerical approach known as a method of approximating functions. It has been suggested in Refs. [5–7] and further developed in the works [8, 9].

The approximating-functions method is a particular case of finite-element method [10], which divides the domain of problem definition by means of a mesh of cells, in each of which a

function under interest is approximated by Lagrange polynomials. Such a technique reduces the problem to solving a system of nonlinear algebraic equations by a standard Newton method [11].

Within the approximating-functions method, the process of solving an external problem (i.e., calculating reflected and transmitted fields outside inhomogeneous region in a medium) is based on sequential computation of these fields at all mesh points outside the interval of inhomogeneity. Note that some of the relations used in this process, although demanding intense use of computational facilities, are common. Their influence increases significantly with increasing degree of nonlinearity of the relations used for polarization.

Separation of such common parts of the problem and calculating them in advance would reduce consumption of computer resources and increase computational performance of the approximating-functions method. Identifying such parts of the problem and developing the ways to calculate them efficiently is the main goal of this study.

2. Problem statement

According to the Volterra integral-equation technique [3, 4], the subject is the integral equation that describes electromagnetic processes in a one-dimensional space-and-time domain [5]:

$$E(\tau,\xi)=E_0(\tau,\xi)-\frac{1}{2}\frac{\partial}{\partial\tau}\left[\int_{\tau_{\min}^{L}}^{\tau}\left(\frac{1}{\varepsilon\varepsilon_0}P(\tau',\xi-\tau+\tau')-\frac{\varepsilon-1}{\varepsilon}E(\tau',\xi-\tau+\tau')\right)d\tau'\right.$$
$$\left.+\int_{\tau_{\min}^{H}}^{\tau}\left(\frac{1}{\varepsilon\varepsilon_0}P(\tau',\xi+\tau-\tau')-\frac{\varepsilon-1}{\varepsilon}E(\tau',\xi+\tau-\tau')\right)d\tau'\right]. \quad (1)$$

Here $E(\tau,\xi)$ is the electric field inside or outside an inhomogeneity located in the area defined by $(\tau,\xi)\in[0,\infty)\times[0,1]$ in a material medium $(\tau,\xi)\in[0,\infty)\times[-\infty,+\infty]$, $E_0(\tau,\xi)$ the initial electric field with no inhomogeneity, $P(\tau,\xi)$ denotes the polarization of medium located inside the inhomogeneity region, which has different electromagnetic characteristics than those of the environment located outside of the interval [0, 1], ε is the permittivity of the environment, and ε_0 the permittivity of vacuum. In Eq. (1), τ' stands for the integration variable in the time domain, while the integration limits are given by $\tau_{\min}^{L}=\max(0,\tau-\xi)$ and $\tau_{\min}^{H}=\max(0,\tau+\xi-1)$. For convenience, dimensionless variables $\tau=vt/L$ and $\xi=x/L$ are introduced, with $v=c/\sqrt{\varepsilon}$, c being the light velocity in vacuum, L the spatial width of inhomogeneity region, and x and t denoting dimensional space and time variables, respectively.

The nonlinearity is introduced into Eq. 1 by means of the features of a material layer, which are described by the polarization written in a brief form as follows:

$$P(\tau,\xi)=\sum_{i=1}^{n}\gamma_i E^i(\tau,\xi). \quad (2)$$

Here the linear properties of the medium inside inhomogeneity region are described by the parameter $\gamma_1=\varepsilon_0(\varepsilon_1-1)$ and the relevant permittivity ε_1, and the nonlinear properties of the *i*-th order ($i\geq 2$) are defined by the nonlinear susceptibilities γ_i.

Eq. 1 describes an internal problem (i.e., a problem inside the inhomogeneity region) whenever a given point belongs to the interval $\xi\in[0,1]$. Outside of this interval, Eq. 1 represents

a quadrature formula for calculating the external field through the internal one. As above, the latter for convenience is termed as the 'external problem'. In the latter case, new upper limits lying outside the inhomogeneity region are used: $\tau_{\max}^{L} = \tau - \xi + 1$ and $\tau_{\max}^{H} = \tau + \xi$, which refer respectively to the first and second integrals. These upper limits are determined by the point of intersection of the integration line for the first (or the second) integral with the upper (or the lower) inhomogeneity boundary for the transmitted (or the reflected) wave. In fact, they are equal to the lower limits increased by the inhomogeneity width.

3. Introduction of general expressions for the external problem

To continue, let us introduce the functions for the first and second parts of Eq. 1 with the upper limits $\tau_{\max}^{L}$ and $\tau_{\max}^{H}$:

$$\begin{aligned} J_L(\tau,\xi,F) &= \frac{\partial}{\partial\tau}\int_{\tau_{\min}^{L}}^{\tau_{\max}^{L}} F(\tau',\xi-\tau+\tau')\,d\tau', \\ J_H(\tau,\xi,F) &= \frac{\partial}{\partial\tau}\int_{\tau_{\min}^{H}}^{\tau_{\max}^{H}} F(\tau',\xi+\tau-\tau')\,d\tau', \end{aligned} \tag{3}$$

where

$$\begin{aligned} F(\tau,\xi) &= \sum_{i=1}^{n}\tilde{\gamma}_i E^i(\tau,\xi), \\ \tilde{\gamma}_i &= \begin{cases} (\varepsilon_1-\varepsilon)/\varepsilon, & i=1 \\ \gamma_i/(\varepsilon\varepsilon_0), & i>1 \end{cases}. \end{aligned} \tag{4}$$

The general relation for calculating the reflected and transmitted fields is as follows:

$$E(\tau,\xi) = E_0(\tau,\xi) - \frac{1}{2}\left[J_L(\tau,\xi,F) + J_H(\tau,\xi,F)\right]. \tag{5}$$

The difference between the cases of calculating the two different fields consists in inclusion (or omission) of some terms: the reflected field lacks the first term $E_0(\tau,\xi)$ and J_L, while the transmitted one lacks J_H. Then the final expressions are given by

$$E_{refl}(\tau,\xi) = -\frac{1}{2}J_H(\tau,\xi,F), \tag{6}$$

$$E_{trans}(\tau,\xi) = E_0(\tau,\xi) - \frac{1}{2}J_L(\tau,\xi,F). \tag{7}$$

4. Modification of approximating-functions method

According to the approximating-functions method [5] adopted to solving Eq. 1, we construct a mesh of semi-closed squares in the time-and-space rectangle, with the side *h* of the square:

$$D_{ij} = \{ih \le \tau < (i+1)h,\ jh \le \xi < (j+1)h\},\ i=\overline{0,\text{n-1}},\ j=\overline{0,\text{m-1}}, \tag{8}$$

where $\mathbf{T}$ denotes a constant (a time limit), whereas $n = \lfloor \mathbf{T}/h \rfloor$ and $m = \lfloor 1/h \rfloor$ are some constants that depend upon the sizes *D* and *h*.

Solution to Eq. 1 can be constructed approximately as a sum of piecewise-smooth functions $\hat{E}_{i,j}(\tau,\xi)$ each of which is determined in the corresponding grid cell D_{ij}:

$\hat{E}(\tau,\xi)=\sum_{i=0}^{n-1}\sum_{j=0}^{m-1}\hat{E}_{i,j}(\tau,\xi)$. These functions are constructed from the four approximating polynomials $\hat{E}_{i,j}(\tau,\xi)=\sum_{d_1=0}^{1}\sum_{d_2=0}^{1}c_{i+k,j+l}\cdot T_{i,j}^{d_1,d_2}(\tau,\xi)$ with the corresponding weighting coefficients $c_{i,j}$, where the approximating polynomials T can be represented in the form of Lagrange polynomials of the second order. They are continuous with their first derivatives on the borders of cells [5].

For the external problem, the reflected and transmitted fields are represented in a similar form:

$$\begin{aligned}\hat{E}_{refl}(\tau,\xi)&=\sum_{i=0}^{n-1}\sum_{j=m_{ref}}^{-1}\hat{E}_{i,j}^{refl}(\tau,\xi),\\ \hat{E}_{trans}(\tau,\xi)&=\sum_{i=0}^{n-1}\sum_{j=m}^{m_{trans}-1}\hat{E}_{i,j}^{trans}(\tau,\xi),\end{aligned}\tag{9}$$

where m_{ref} and m_{trans} are the minimal and maximal magnitudes of the spatial variable in the index units, and $\hat{E}_{i,j}^{refl}(\tau,\xi)$ and $\hat{E}_{i,j}^{trans}(\tau,\xi)$ have the same form as $\hat{E}_{i,j}(\tau,\xi)$. The final relations for calculating the external-problem fields at the mesh points (see Eqs. (6) and (7)) read as

$$\hat{E}_{refl}(\tau_i,\xi_j)=-\frac{1}{2}\hat{J}_H(\tau_i,\xi_j),\tag{10}$$

$$\hat{E}_{trans}(\tau_i,\xi_j)=E_0(\tau_i,\xi_j)-\frac{1}{2}\hat{J}_L(\tau_i,\xi_j),\tag{11}$$

where $\hat{J}_{L,H}(\tau,\xi)=J_{L,H}(\tau,\xi,\hat{F})$, while $\hat{F}$ is given by Eq. (4) and depends on the approximating function $\hat{E}(\tau,\xi)$.

5. Separation of common blocks in the expressions

The form of kernel of Eq. (5) ensures equality of the J_L or J_H values at all the points of each integration path (a 'diagonal' line) of the time-space domain of integration (e.g., in all 'diagonal' lines shown in Fig. 1). Let us prove this for the case of J_L. Denote the integral and the integration limits in J_L respectively as

$$\Phi(\tau-\xi)=\int_{f_1(\tau-\xi)}^{f_2(\tau-\xi)}F(\tau',\xi-\tau+\tau')d\tau',\tag{12}$$

$$f_1(\tau-\xi)=\tau_{\min}^{L}=\max(0,\tau-\xi),\ f_2(\tau-\xi)=\tau_{\max}^{L}=\tau-\xi+1.\tag{13}$$

Then one can rewrite J_L as

$$J_L(\tau,\xi,F)=\frac{\partial}{\partial\tau}\Phi(\tau-\xi)=\frac{\partial\Phi(\tau-\xi)}{\partial(\tau-\xi)}\frac{\partial(\tau-\xi)}{\partial\tau}=\frac{\partial\Phi(\tau-\xi)}{\partial(\tau-\xi)}.\tag{14}$$

Hence, J_L is a constant at all the points where the conditions $\tau-\xi=\text{const}$ and $\xi\geq 1$ are valid (i.e., on the boundary $\xi=1$ and further on), e.g. at the points A, B, C and D in Fig. 1. These points represent the lines parallel to the line $\xi=\tau+1$ (see a dashed line on the left side in Fig. 1). This also means that the transmitted field is zero at the points $\xi\geq\tau+1$ (i.e., in the area N on the left side in Fig. 1), since in this case the upper limit $\tau_{\max}^{L}$ in the integral given by Eq. (12) is always non-positive.

The proof for the case of J_H integral is the same as for J_L. In other words, the J_H value remains constant at all the points where we have $\tau + \xi = \text{const}$ and $\xi \le 0$ (i.e., in front of the inhomogeneity region and on the boundary itself, $\xi = 0$). In fact, these are the lines parallel to the line $\xi = -\tau$ (see a dashed line on the right side in Fig. 1). The reflected field is zero at the points $\xi \le -\tau$ (i.e., in the area N on the right side in Fig. 1) since the upper limit $\tau_{\max}^{H}$ has always a non-positive value.

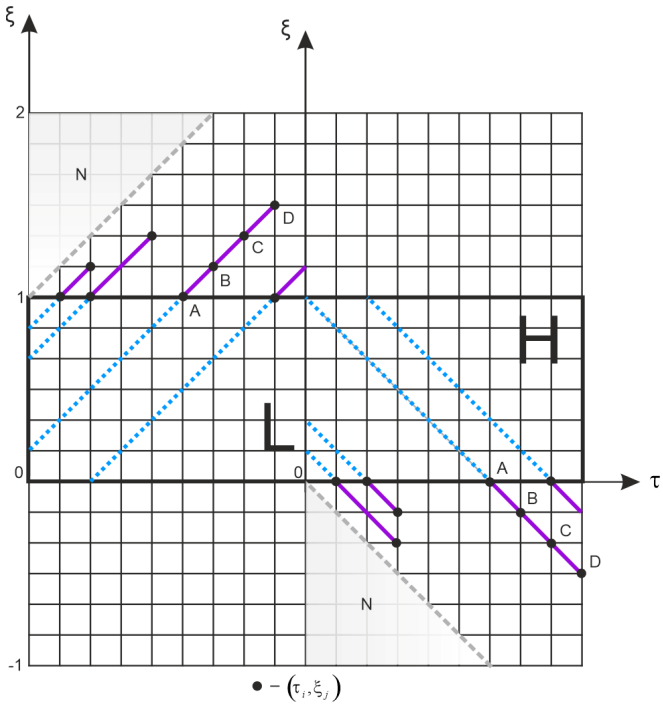

Fig. 1. Integration paths used for calculating integrals J_L (left) and J_H (right) in the same one-dimensional space-and-time area $(\tau, \xi) \in [0, \infty] \times [-1, 2]$. Solid lines correspond to the regions where the integrals have a constant value, dotted lines complement the corresponding solid lines to the opposite boundaries $\xi_b \in \{0,1\}$ of the layers $\xi \in [0,1]$ (they are introduced for convenience only), N denotes the area where the integrals have a zero value, and A, B, C and D are some points lying on a 'diagonal' line.

According to the above analysis, the following must be done in order to build a more efficient scheme for calculating the reflected and transmitted fields in the frame of the approximating-functions method: (i) the areas of zero-field values should be excluded from the calculation process and (ii) one has to calculate J_L at the points $(\tau, 1)$ only one time (for the transmitted field) and J_H at the points $(\tau, 0)$ (for the reflected field), and then save the appropriate results.

Furthermore, the known field $\hat{E}$ on the inhomogeneity boundaries $\xi_b \in \{0,1\}$ can give us the approximated $\hat{J}_L$ and $\hat{J}_H$ values at any mesh points (i, j_b) ($j_b \in \{0, m\}$). Indeed, Eq. (5) in this case has a known left part $\hat{E}(\tau_i, \xi_b)$, a known initial field $E_0(\tau_i, \xi_b)$ and only one integral ($\hat{J}_L$ or $\hat{J}_H$), because the other integral is equal to zero on the appropriate boundary (e.g., $\hat{J}_L$ is zero on the boundary $\xi_b = 0$ and $\hat{J}_H$ on the boundary $\xi_b = 1$). Therefore, one can simply calculate the

$\hat{J}_{L,H}\left(\tau_i,\xi_b\right)$ values ($i=\overline{0,n}$) and then find the final reflected and transmitted fields, using Eqs. (10) and (11).

The resulting external-problem fields at the discrete mesh points read as

$$\hat{E}_{refl}\left(\tau_i,\xi_j\right)=\hat{E}\left(\tau_i+\xi_j,0\right)-\hat{E}_0\left(\tau_i+\xi_j,0\right), \tag{15}$$

$$\hat{E}_{trans}\left(\tau_i,\xi_j\right)=\hat{E}_0\left(\tau_i,\xi_j\right)+\hat{E}\left(\tau_i-\xi_j,m\right)-\hat{E}_0\left(\tau_i-\xi_j,m\right). \tag{16}$$

The final formulae for calculating the coefficients $c_{i,j}$ of polynomials entering Eq. (9) are as follows:

$$\begin{aligned} c_{i,j} &= \hat{E}_{i+j,0}-\hat{E}^0_{i+j,0}, && j\le 0,\\ c_{i,j} &= \hat{E}^0_{i,j}+\hat{E}_{i-j,m}-\hat{E}^0_{i-j,m}, && j\ge m. \end{aligned} \tag{17}$$

Here $E^0_{i,j}=E_0\left(\tau_i,\xi_j\right)$ (with $i=\overline{0,n}$ and $j=\overline{m_{ref},m_{trans}}$) represents a tabular definition of the initial-field function, with its values defined at the points of the mesh *D*. Depending on its type, preliminary computation of this table can increase drastically the computation speed, if compared with any real-time computations in Eq. (17) (e.g., as it has been described in Refs. [7, 12]).

The final relations given by Eq. (17) contain only simple arithmetic operations, which are the fastest in the calculations performed on computer software (see, e.g., Ref. [13]). Due to independent calculations of the transmitted and reflected fields at each point outside of the inhomogeneity region, the computational process can be efficiently performed in parallel, which also boosts the speed and saves RAM and other computer resources. Moreover, the independence mentioned above enables building this process in a fault-tolerant way, thus saving each execution result on a fault-tolerant storage resource, like it has been described in Refs. [7, 14]. Finally, this circumstance makes it easy to stop or start the algorithm after any manual or accidental shutdown.

6. Validation of the approach

Now we will test the accuracy of our technique for a particular case of nonlinear problems and compare its computational speed with that typical for unmodified version of the method. A particular example used by us is the problem of Gaussian pulses passing through a layer with quadratic nonlinearity described by Eq. (2). Here the nonlinear parameter of the layer is $\gamma_2=1$, unless otherwise is stated. We use the electromagnetic parameters $\varepsilon_1=11$ and $\varepsilon=9$ respectively for the surrounding medium and the layer. The modelling time interval is $\tau\in\left[0,10\right]$ and the wave propagation starts from the point $\xi_b=0$.

The correctness of our solution has been checked using the two indicators. The first one is field continuity that must take place on the boundaries of the layer. This condition is represented by the approximate equalities $E_0\left(\tau,0\right)+\hat{E}_{refl}\left(\tau,0\right)-\hat{E}\left(\tau,0\right)\approx 0$ and $\hat{E}_{trans}\left(\tau,1\right)-\hat{E}\left(\tau,1\right)\approx 0$ respectively for the left-hand and right-hand boundaries. The second indicator is energy balance that can be checked using the relations taken from Ref. [5].

First we model a simple Gaussian pulse $E\left(\tau,\xi\right)=\exp(-\left(\tau-\tau_0-\xi\right)^2/2\sigma^2)$ (with $\tau_0=1$ being the initial time offset and $\sigma=0.1$), using the mesh step $h=0.02$. Multiple reflections occurring from the layer boundaries and pulse broadening appearing due to nonlinearity of the layer medium can be clearly seen from Fig. 2. Hereafter, we do not represent the incident wave in the figures in order to visualize better the reflected wave.

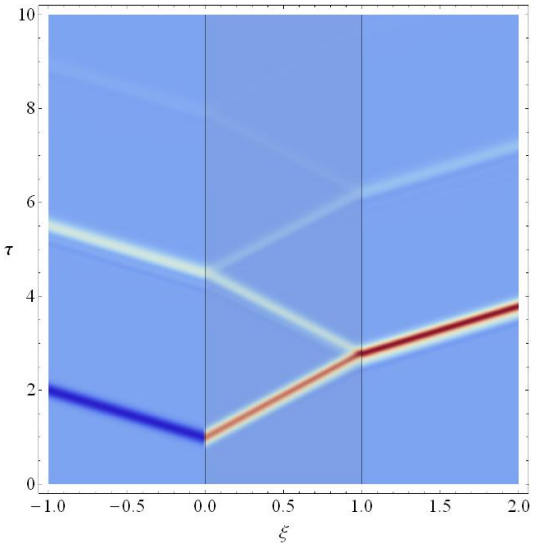

Fig. 2. Transformation of a simple Gaussian pulse by a material medium with quadratic nonlinearity (see the text). The process starts on the left boundary $\xi_b = 0$ at the moment $\tau = 1$. Left and right sides of the figure correspond to evolution of the reflected and transmitted fields, respectively, while its middle part refers to evolution of the field inside the layer with inhomogeneity.

The amplitude of the wave decreases from positive (a red colour in Fig. 2) to negative (a blue colour) values through a zero (a background colour). Here and below, it is understood that, under influence of the layer, the wave amplitude inside the layer is much less than those of the incident and transmitted waves. In what the first indicator is concerned, the maximal error is equal to 8.41×10^{-3}% and the median is 7.35×10^{-4}%. The maximum of energy-flow imbalance amounts to 6.81%, with the median 1.63%. This agrees well with the results reported in Refs. [5, 15]. However, the speed of our calculations of the external problem has increased by 26 times, even though the approaches [12] have been always employed for increasing the computations speed by caching the results obtained for the working relations. The reason is a large difference in complexity of the original relations and those suggested in the present work.

Another pulse $E(\tau,\xi) = -(\tau-\tau_0-\xi)/\sigma^2 \exp(-(\tau-\tau_0-\xi)^2/2\sigma^2)$ has been modelled, using the nonlinear parameter $\gamma_2 = 0.3$ of the layer and the mesh step $h = 0.005$. The data of Fig. 3 testifies still more beam diffusion after each reflection from the layer boundaries and distortion of pulse shape occurring due to nonlinearity of the layer medium. Under influence of the layer, the wave energy is redistributed in time and, after each reflection, the pulse shape becomes more and more similar to that of an Airy pulse [16]. Besides, the speed of wave propagation in the layer slows down. Concerning the first indicator, the maximal error is equal to 2.34×10^{-4}% and the median value to 1.15×10^{-5}%. The appropriate energy-flow imbalance maximum is 6.1%, with the median 1.03%.

Finally, we have modelled the pulse $E(\tau,\xi) = \cos(\eta(\tau-\tau_0-\xi))\exp\left(-(\tau-\tau_0-\xi)^2/2\sigma^2\right)$ with the normalized frequency $\eta = 10$ and the mesh step $h = 0.005$ (see Fig. 4). The speed of the wave propagation in the layer slows down, too. The reflected wave and, especially, the transmitted wave lose the initial structure of the incident wave and acquire a 'sawtooth' shape. The wave propagation in Fig. 4 starts from the point $\xi = -1$ for easier observation of decreasing rate for the wave amplitude after each re-reflection inside the layer. The maximal error for the first indicator is equal to 3.18×10^{-4}% and the median to 1.01×10^{-6}%. Finally, the maximal energy-flow imbalance amounts to 5.23%, with the median 1.07%.

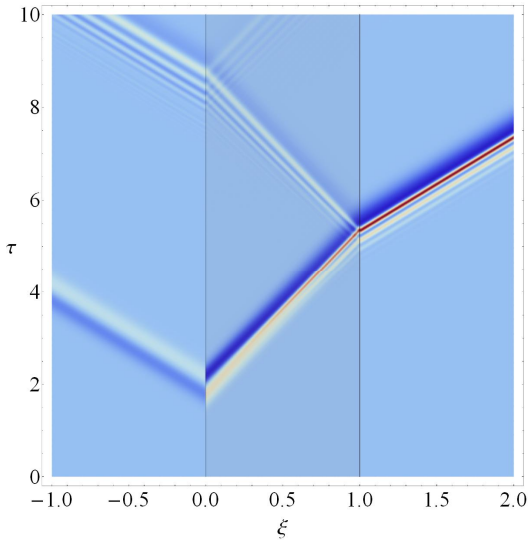

Fig. 3. Transformation of single-cycle Gaussian pulse by a material medium with quadratic nonlinearity (see the text). The process starts on the left boundary $\xi_b = 0$ at the moment $\tau = 1$. Left and right sides of the figure correspond to evolution of the reflected and transmitted fields, respectively, while its middle part refers to evolution of the field inside the layer with inhomogeneity.

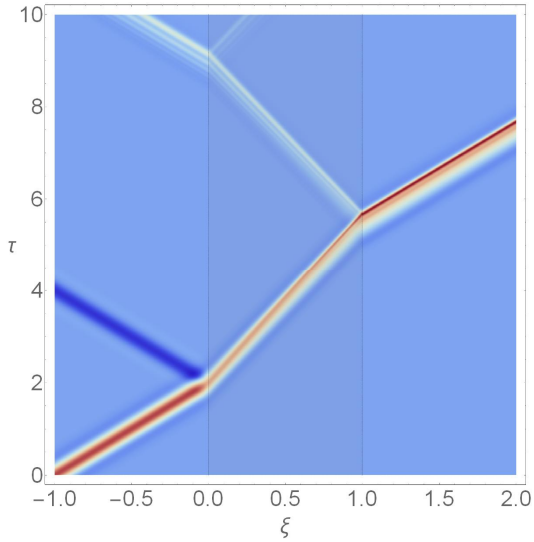

Fig. 4. Transformation of a multiple-cycle Gaussian pulse by a material medium with quadratic nonlinearity (see the text). The process starts at $\xi = -1$ from the left at the moment $\tau = 0$. Left and right sides of the figure correspond to evolution of the reflected and transmitted fields, respectively, while its middle part refers to evolution of the field inside the layer with inhomogeneity.

7. Conclusions

We have developed the approach to improve the computational efficiency of the approximating-functions method, which is based upon the Volterra integral-equation approach. It can be successfully applied when solving one-dimensional space-and-time electrodynamics problems of nonlinear material media. In the frame of this method, one replaces the process of calculating the reflected and transmitted fields lying in front and behind the inhomogeneity region in a medium by a much simpler algorithm and simple relations. The algorithm modified in this manner still remains mathematically equivalent to the original version of the method.

We have proved that, in order to determine the field outside of the inhomogeneity region, it is necessary to know only the field values at its boundaries and the initial field outside. The former fields can be obtained when solving the problem inside the inhomogeneity region, whereas the latter field can be calculated in real time – or calculated in advance and then stored. To solve the problem, one still has to calculate the initial field outside of the inhomogeneity region. This means that there is no additional computational load when we apply the approach developed in the present work. The process suggested by us for computing the outside field exploits pre-computed

values for specific mesh points, instead of permanently evaluating some complex expressions. This efficiently saves RAM and other computer resources.

Our final numerical–analytical relations contain only simple arithmetic operations, which are the fastest for the calculations based on computer software. Due to independence of the calculation of the outside fields at each mesh point, the computing process can be efficiently done in parallel. This enables building it in a fault-tolerant way, which makes easy stopping or starting the algorithm after any manual or accidental shutdown.

We have applied our approach to solve a number of specific physical problems. These are transformations of different Gaussian-like pulses by a material layer manifesting second-order nonlinear properties. The estimation of calculation errors reveals high efficiency of our method. Namely, the speed of calculations of these known problems has been increased by 26 times. Of course, the actual rate of increase in the speed in any practical situation would also depend on the nonlinearity of medium in the inhomogeneity region, the time interval under test, the number of parallel threads employed during computations, the programming language, and some other characteristics of a computing system.

References

1. Shifman Y and Leviatan Y, 2001. On the use of spatio-temporal multiresolution analysis in method of moments solutions of transient electromagnetic scattering. IEEE Trans. Anten. Propag. **49**: 1123–1129.
2. Gomez M R, Salinas A and Bretones A R, 1992. Time-domain integral equation methods for transient analysis. IEEE Anten. Propag. Mag. **34**: 15–24.
3. Nerukh A G, Sakhnenko N K, Benson T and Sewell P. Non-stationary electromagnetics. New York: Jenny Stanford Publishing Ltd., 2012.
4. Nerukh A and Benson T. Non-stationary electromagnetics: An integral equations approach (2nd ed.). Boca Raton: Jenny Stanford Publishing, 2018.
5. Nerukh A, Zolotariov D and Benson T, 2015. The approximating functions method for nonlinear Volterra integral equations. Opt. Quant. Electron. **47**: 2565–2575.
6. Zolotariov D and Nerukh A, 2011. Extension of the approximation functions method for 2D non-linear Volterra integral equations. Appl. Radioel. **10**: 39–44.
7. Zolotariov D, 2021. The new modification of the approximating functions method for cloud computing. Int. J. Math. Comp. Res. **9**: 2376–2380.
8. Anish D, Dasgupta A and Sarkar G, 2006. A new set of orthogonal functions and its application to the analysis of dynamic systems. J. Franklin Inst. **343**: 1–26.
9. Maleknejad K, Almasieh H and Roodaki M, 2010. Triangular functions (TF) method for the solution of nonlinear Volterra–Fredholm integral equations. Commun. Nonlin. Sci. Numer. Simul. **10**: 10–12.
10. Ern A and Guermond J-L. Finite elements I: Approximation and interpolation. Cham: Springer International Publishing, 2021. https://doi.org/10.1007/978-3-030-56341-7
11. Deuflhard P. Newton methods for nonlinear problems. Springer, 2011. Zolotariov D, 2020. The methods for iterative computations efficiency improving in Wolfram Mathematica. Bionics of Intelligence. **95**: 63–68.
12. Zolotariov D, Nerukh A. The approximating functions method for Volterra integral equations: implementation of a computational experiment in nonstationary electrodynamics. Lambert Academic Publishing, 2011.

13. Zolotariov D, 2022. Design of hardware and software complex of fault-tolerant computing by iterative methods. Amer. J. Engineer. Res. **11**: 06–11.
14. Zolotariov D and Nerukh A, 2013. Transformation of Gaussian-like pulses by a nonlinear dielectric layer. European Microwave Conference. Nuremberg, 2013. P. 1251–1254.
15. Nerukh A G, Zolotariov D A and Nerukh D A, 2012. Properties of decelerating non-diffractive electromagnetic Airy pulses. Appl. Radio Electron. Sci. Mag. **11**: 77–83.

Zolotariov D. 2022. Improvements in approximating-functions method for the optical reflection and transmission problems of nonlinear dielectric layers. Ukr.J.Phys.Opt. **23**: 86 – 95.
doi: 10.3116/16091833/23/2/86/2022

Анотація. *Удосконалено відомий метод апроксимуючих функцій, який є частковим випадком методу скінченних елементів, із метою розв'язування електродинамічних задач оптичного відбивання та пропускання одновимірного шару в часовій області, використовуючи методику інтегрального рівняння Вольтерра. Основною метою цього вдосконалення є підвищення швидкості обчислень і пониження витрат ресурсів комп'ютера, що особливо важливо для задач нелінійних середовищ. Метод перевірено на прикладі проблем відбивання та пропускання, що виникають для трьох різних типів електромагнітних ґаусових імпульсів, які падають на шар матеріалу з нелінійністю другого порядку, вставленим поміж лінійними середовищами.*